Review of Scientific Instruments

Enhanced bandwidth, high gain, low noise transimpedance amplifier for asynchronous optical sampling systems

Cite as: Rev. Sci. Instrum. **90**, 063103 (2019); https://doi.org/10.1063/1.5089117
Submitted: 16 January 2019 . Accepted: 18 May 2019 . Published Online: 11 June 2019

Xue Yang, Bo Su, Yaxiong Wu, Hongfei Zhang, and David R. Jones

View Online Export Citation CrossMark



© 2019 Author(s).

Review of Scientific Instruments ARTICLE scitation.org/journal/rsi

Enhanced bandwidth, high gain, low noise transimpedance amplifier for asynchronous optical sampling systems

Cite as: Rev. Sci. Instrum. 90, 063103 (2019); doi: 10.1063/1.5089117
Submitted: 16 January 2019 • Accepted: 18 May 2019 •
Published Online: 11 June 2019

View Online Export Citation CrossMark

Xue Yang, Bo Su,[a] Yaxiong Wu, Hongfei Zhang, and David R. Jones

AFFILIATIONS

Key Laboratory of Terahertz Optoelectronics, Ministry of Education, Beijing Key Laboratory for Terahertz Spectroscopy and Imaging, Beijing Advanced Innovation Centre for Imaging Theory and Technology, Department of Physics, Capital Normal University, Beijing 100048, China

[a]Author to whom correspondence should be addressed: su-b@163.com

ABSTRACT

The methodology to correctly identify the high-bandwidth devices that are able to deliver the lowest noise voltage-amplification from receiving terahertz antenna or photodiode current sources is detailed. We further show that to achieve the lowest noise levels, amplifier input capacitance must be minimized requiring the amplifier and detection circuitry to be carefully integrated. We validate a useful technique to minimize feedback parasitic capacitance and demonstrate a transimpedance amplifier (TIA) with a peak gain of 100 MΩ, 0.5 MHz bandwidth, and a signal power to noise power ratio (SNR) of 23 dB for a 5 nA peak-current input and outline the steps required to increase this to 50 dB. Employing this TIA on a 1550 nm fiber-based terahertz asynchronous optical sampling system realizes a 700 mV, 26 dB SNR, single-scan signal from the 8 nA peak/peak antenna source and removes the requirement for an additional data acquisition trigger signal. Real time, subsecond terahertz data collection is possible at a SNR of 30 dB averaging over 16 scans.

Published under license by AIP Publishing. https://doi.org/10.1063/1.5089117

I. INTRODUCTION AND MOTIVATION

The pump-probe technique is a valuable tool for studying ultrafast electronic dynamics, where an ultrashort laser pulse is divided between a pump beam, to excite a sample and generate a nonequilibrium state, and a probe beam used to monitor the pump-induced changes. Measuring changes in optical constants as a function of the time delay between the arrival of the pump and probe pulses yields information on the sample. The time delay between the pump and probe pulse is most commonly achieved by slow scanning of a mechanical translation stage achieving time delays of nanoseconds before the scan period becomes too onerous. Vibrating, rotational, and other types of stages have been proposed[1–3] for rapid scanning, but here the time delay is limited to a few tens of picoseconds, restricting the investigation of the optoelectrical response over long time scales as well as applications where high frequency resolution is required. Conventional terahertz time-domain spectroscopy (THz-TDS) is a typical application of the pump-probe technique. Mode locked femtosecond laser pulses are divided to generate and detect terahertz radiation. High spectral resolution requires wide time windows, imposing large scanning ranges and long acquisition times.

Asynchronous optical sampling (ASOPS) is a novel technique[4,5] that employs two phase locked ultrafast laser sources as the pump and probe beams operating at a pulse repetition frequency (PRF) f_0 and $f_1 = f_0 - \Delta f$, respectively. The principle is displayed pictorially in Fig. 1.

The frequency difference, Δf, enables fast scanning of temporal delays from 0 to $\tau = 1/f_0$ accomplished in time, $t = 1/\Delta f$, without mechanical motion. The real time, t, can be converted to the scan time delay, τ, by $\tau(t) = t \times \Delta f/f_0$. The time resolution is

$$\Delta\tau = 1/f_0 - 1/f_1 = \Delta f/f_0 f_1. \quad (1)$$

Terahertz-ASOPS systems typically employ lasers in the 0.1–1 GHz PRF range, giving a scan range of 10–1 ns, and are theoretically capable of achieving high frequency resolution within an acceptable data acquisition period. However, if the effective bandwidth of the data acquisition electronics, F, is lower than the laser PRF, this time

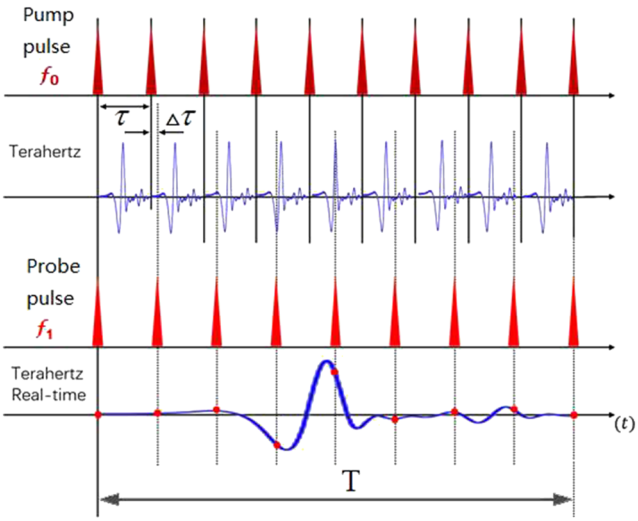


FIG. 1. Time-delay principle of the ASOPS scheme.

resolution limit becomes[6]

$$\Delta\tau' = \Delta f/f_0 F. \quad (2)$$

However, unlike conventional THz-TDS, where the scan time delay is known within the error of the mechanical stage, THz-ASOPS systems are subject to an additional time resolution limit owing to timing error arising from within the control electronics. A common scheme to achieve a locked difference frequency, Δf, requires both lasers stabilized to individual synthesizers sharing a common 10 MHz reference oscillator, with the difference frequency set by the synthesizers. For a nominal 1 GHz THz-ASOPS system, a time-delay resolution of 280 fs was initially obtained at a Δf = 10 kHz.[6] This scheme was limited by phase-noise intrinsic to the synthesis process of each synthesizer. Reducing Δf to 1 kHz, lower frequency phase-noise contributions of the synthesizers degraded the time-delay resolution to greater than 1 ps.[6] Improved time-delay resolution to 160 fs[7] and then to 45 fs[8] was obtained by operating the phase-locked loop electronics at the third and then the tenth harmonic of the repetition frequency, respectively. In both cases, the feedback loop was able to perform a tighter offset lock with a reduced timing jitter due to enhanced phase-noise sensitivity. These results were achieved in conjunction with removing the common reference oscillator and slaving one of the laser's PRFs to the other free running laser, removing one feedback loop. Consequently, only the noise floor of one feedback loop is present and uncorrelated phase noise between the two individual synthesizers does not affect the time-delay resolution.[7,8] Finally, the frequency shifter used to define the offset frequency was replaced by direct-digital synthesis (DDS) electronics allowing for a better calibration of the time-delay axis.[8] Here, a 45 fs time resolution was achieved at a Δf of 2 kHz which is the femtosecond laser pulse duration limit. Dropping to a Δf of 1 kHz, no deterioration in timing error was observed over the first 500 ps scan delay. These techniques are applicable to fiber based ASOPS systems; however, as a consequence of Eq. (2) and the reduced PRF (<150 MHz) typical of these systems, a reduced time resolution for a given offset frequency is encountered. Reducing Δf to compensate competes with an increase in the timing-delay error generated within the control electronics[6,9] as discussed above. Time delay resolutions of 67 fs[10] at 1 kHz Δf and 278 fs[11] at 100 Hz Δf have been reported on 100 MHz PRF ASOPS systems which extrapolate to a time delay resolution of ~400 fs at a typical Δf of 20 Hz employed on these systems.[6,10,11]

For all THz-ASOPS systems, the high detection bandwidth (typically very much greater than 100 kHz) required to achieve high temporal resolution precludes the use of Lock-In-Amplifier (LIA) techniques to extract the terahertz signal from within the noise. Instead, acquired signals are averaged over multiple time scans to remove incoherent noise. The requisite trigger signal to initiate each data acquisition sweep can be obtained directly from the control electronics[6] or, optically, via interferometric[12] and two photon processes.[13,14] For ultimate resolution, an optically derived trigger signal is preferred as the timing error between multiple scans may be minimized close to the signal.

For THz-ASOPS systems, much attention has been paid to improving the scan resolution to take full advantage of the fast scanning over large temporal delays, as detailed above. However, less attention is given on information presented concerning the initial amplification of the terahertz signal beyond quoting the detection bandwidth. Noise reduction and hence achieving the required signal to noise ratio (SNR) is accomplished by high signal averaging and correspondingly long acquisition times extending over many tens or even hundreds of seconds.[8,9] Here, we show that careful attention to the detection and amplification circuitry can increase both the bandwidth of the amplifier circuitry and the signal to noise ratio and, as a consequence, result in improved resolution and significantly reduced signal averaging time.

II. PRINCIPLE

Detection of terahertz signals occurs directly from a receiving terahertz antenna[12] or indirectly via a photodiode.[8] Both may be considered as current sources; requiring a front-end transimpedance amplifier (TIA) to initially convert the current source to an amplified voltage signal, thereafter cascaded voltage amplification stages may be added to achieve the required signal voltage-magnitude and total circuit bandwidth. Figure 2 displays a TIA circuit in schematic.

To compare the signal and noise level of the circuit, it is convenient to examine the circuit noise as an "input referred noise,"

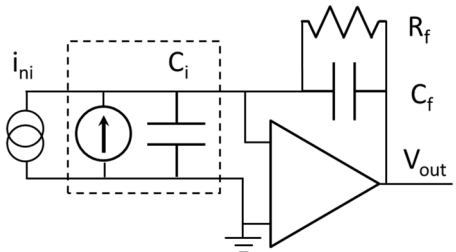


FIG. 2. Transimpedance amplifier circuit, feedback resistor R_f with parasitic capacitance C_f, C_i is the current source internal parallel capacitance, and I_{ni} is the input referred to noise (see text).

Published under license by AIP Publishing

TABLE I. Opamp parameter values.

	OPA657	LMH6629	LTC6268-10
C_{cm} (pF)	0.7	1.7	0.45
C_{dif} (pF)	4.5	4	0.1
GBWP (GHz)	1.65	4	4
i_n (pA/$\sqrt{}$Hz)	0.0013	2.6	0.007
e_n (nV/$\sqrt{}$Hz)	4.8	0.69	4.0

i_{ni}, originating at the opamp input. This enables direct evaluation of both signal power to noise power ratio (SNR) and the discrete noise sources. The expression for i_{ni} is conveniently expressed in Eq. (3) as functions of the circuit and opamp-noise parameters[15]

$$i_{ni} = \sqrt{i_n^2 + \left(\frac{e_n}{R_f}\right)^2 + \frac{4KT}{R_f} + \frac{(e_n 2\pi f_{-3\mathrm{dB}} C_{in})^2}{3}} \tag{3}$$

with $C_{in} = C_i + C_{cm} + C_{dif}$ and $f_{-3\mathrm{dB}} = \sqrt{\frac{GBWP}{2\pi R_f C_{in}}}$, where C_{cm} and C_{dif} are the opamp input common mode and differential mode capacitances, respectively, and GBWP is the "opamp amplifier gain bandwidth product." Finally, i_n is the "inverting input spot current noise" and e_n is the "noninverting input spot voltage noise." The four noise terms, from left to right, are generally denoted as current noise, voltage noise, thermal noise, and input capacitance noise terms. For the ease of reference, the parameter values for three suitable opamps are recorded in Table I. The SNR values are graphed as functions of the −3 dB bandwidth for two values of device capacitance, 10 pF and 1 pF, displayed in Figs. 3(a) and 3(b), respectively, with the values of R_f shown for clarity. Immediately obvious in Fig. 3(a) is the flat-line SNR response of the LMH device at increased gain due to a dominant current noise term, a consequence of its high i_n value. The higher LTC performance compared with the OPA device is due to its greater GBWP. At lower gain values, the input capacitance noise term dominates in the OPA and LTC devices, favoring the LMH6629 due to its low e_n value. However, if a low capacitance device is selected and care is taken to minimize input lead capacitance, then the significantly lower total C_{in} value possible for the LTC device preferentially increases not only the SNR of this device but also its bandwidth for a given value of f_r, as evident in Fig. 3(b). Achieving the highest SNR for a required bandwidth demands attention to both device and opamp selection.

In Fig. 3(a), a value of 5 nA for the current source input is quoted to reflect the typical output from a terahertz receiver antenna driven by 10 mW of average power from a 1550 nm wavelength, nominal 140 fs pulse length, fiber laser operating at the PRF of 100 MHz, such as the system used in the study here. To realize a time resolution of 200 fs (which approaches the 140 fs laser pulse duration limit) for these systems at a Δf of 20 Hz requires a detection bandwidth of 1 MHz and would also realize a 200 fs time resolution at a Δf of 200 Hz for a 1 GHz ASOPS system. This may theoretically be realized employing an LTC6268-10 in a single stage TIA with a feedback resistor value of 100 MΩ and would generate a convenient output voltage of 500 mV at an SNR of 100 dB. However, in practice, this is considered unobtainable due to C_f restricting the feedback impedance. For standard 1206 packaged surface mount resistors on FR-4 board, the quoted minimum parasitic capacitance is ~0.1 pF giving an impedance of 0.8 MΩ at 2 MHz. The total parasitic feedback capacitance must be reduced by at least two orders of magnitude. One obvious solution is to employ multiple feedback resistors in series; in this instance, the feedback impedance, Z, is given by[16]

$$Z = \frac{NR}{1 + sR\left(C_f + NC_{in}\right)}. \tag{4}$$

In practice, the presence of C_{in} and the large number of resistors required dooms; this approach as N is always very much greater than C_f/C_{in} generating a pole at a frequency of $f_r = 1/(2\pi NRC_{in})$ which is inversely proportional to N. Employing multiple feedback resistors in series in this simple approach limits bandwidth improvement to less than a factor of 2.[16] However, an additional technique

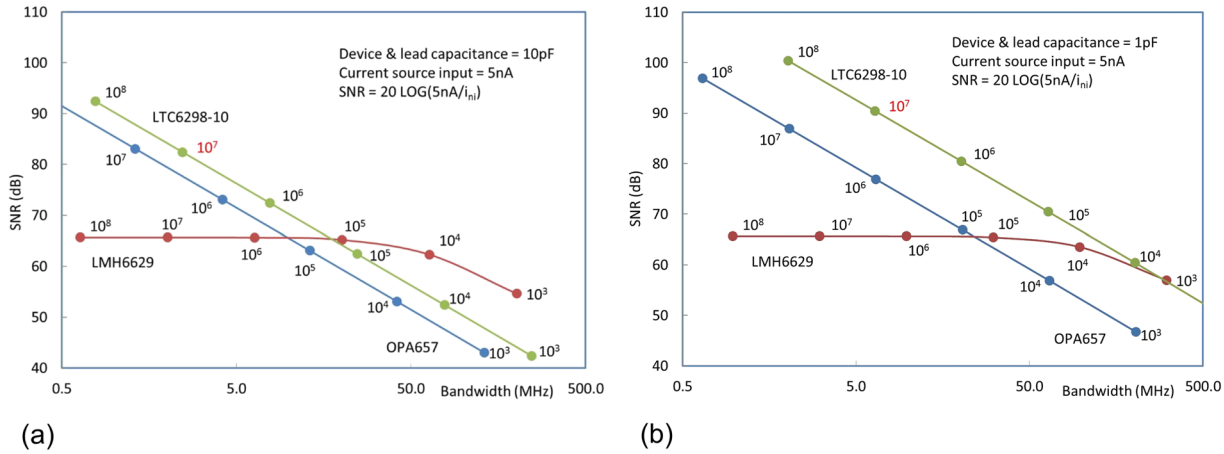


FIG. 3. SNR for three opamps, graphed as a function of bandwidth (see text), (a) C_i = 10 pF and (b) C_i = 1 pF.

Published under license by AIP Publishing

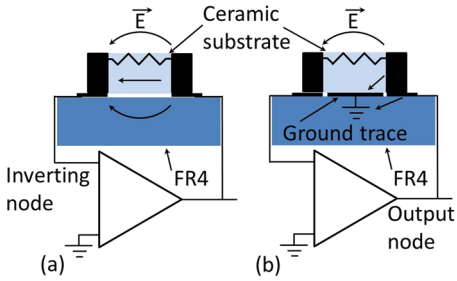


FIG. 4. Standard feedback resistor layout (a) and field shunting layout (b).

to reduce the parasitic capacitance is to shield the E field paths that give rise to the capacitance by placing a ground trace between the resistor pads. Such a ground trace shields the output field from getting to the inverting node of the resistor by shunting the field to ground instead. Figure 4 details the topology of this technique. If the optimistic assumption is made that all field lines are shunted to ground in the dielectric materials and given the 1206 package pad dimensions, an upper limit on the residual parasitic capacitance of 5 fF is obtained through air, corresponding to a 20-fold reduction. This drastically reduces the number of resistors required in the series chain. In addition, careful positioning of the resistors and accompanying ground traces will minimize C_{in}. Finally, the LTC6268-10 S8 package topology is ideally suited for routing the shielding ground traces.

III. TRANSIMPEDANCE AMPLIFIER DESIGN, BOARD LAYOUT, AND GAIN CHARACTERISTICS

For completeness, the full schematic and printed circuit board (PCB) layout, generated on Eagle software, of the double feedback resistor TIA is displayed in Figs. 5(a) and 5(b), respectively. The two-layer design, on standard 1.6 mm thickness FR-4 board, was developed for high frequency (>50 MHz) operation and has proved to be stable with well controlled characteristics. The opamp pin connections are directly transcribed from Figs. 5(a) and 5(b).

The track layouts for the single and double feedback resistor designs are shown in closer detail in Figs. 6(a) and 6(b), respectively. All components are on the upper level with blue-colored blocks denoting the underside ground-plane and red colored blocks denoting the top level ground-plane, likewise blue tracks and red tracks are on the lower and upper levels, respectively.

A track width of 0.6 mm was used for the E-field shunting top and lower ground lines for the single feedback resistor design of Fig. 6(a). For the double feedback resistor design of Fig. 6(b) the lower (blue) track width was increased to 1.2 mm. The pin layout of the LTC device facilitates a straight forward ground-line layout to isolate both the pads of each resistor and the input and output pins of the opamp.

To determine the gain of the TIA device, a 0–20 mV peak/peak variable frequency sign-source was used via a 2 MΩ resistor chain consisting of four 1206 SMA series 500 kΩ resistors mounted in air across the center pins to two SMA coax-connectors and provided a peak current of 10 nA, while restricting the total parasitic capacitance of the chain to 12 fF, assuming a parasitic capacitance per resistor of 50 fF in air (detailed in their specifications). A 0.4 m length RG316 coax cable connected the resistor chain to the TIA input.

The SPICE simulation software "LTspice" was employed to model the amplifier characteristics with the topology and general component values given in Fig. 7. Initial starting capacitances were determined as follows. The capacitance of the top ground trace to the resistor was determined as a 0.6 mm wide, 1.6 mm long, microstrip above a ground plane, with the small addition of the bottom ground plane ignored. This capacitance is distributed and modeled simply by dividing the resistors in two (R3 and R4) and

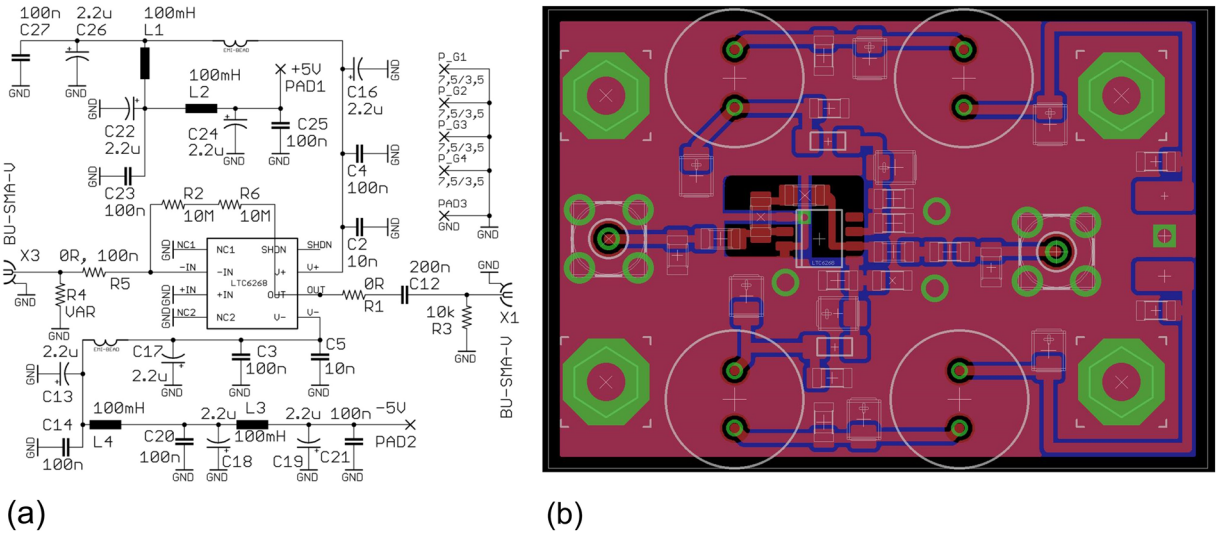


FIG. 5. (a) TIA parts schematic and (b) component layout.

Published under license by AIP Publishing

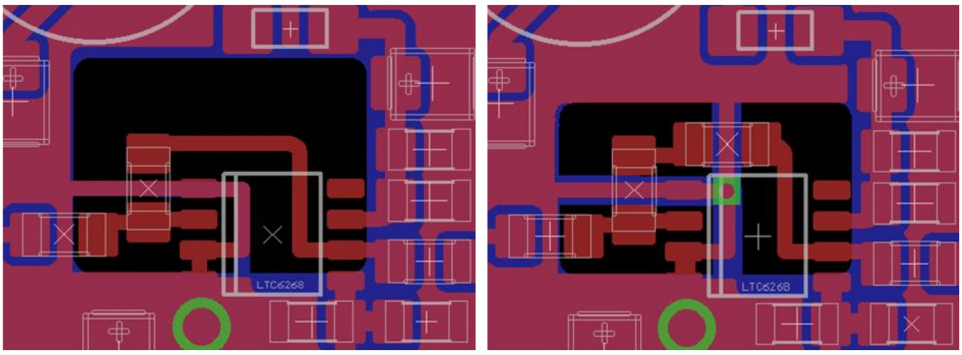


FIG. 6. Expanded view of the single (a) and double (b) feedback resistors, opamp, and E-field shunting ground lines.

placing the three capacitors (C8, C9, and C10) as shown in Fig. 7(a). The top ground trace capacitance to the resistor pads was calculated as 0.6 mm wide coplanar-strips with a dielectric constant of 9 above and 4.4 below. Finally, the bottom 0.6 mm and 1.2 mm wide ground strip capacitances to the resistor pads were calculated as off-axis capacitors; the pad capacitances are given by C6 and C7 in Fig. 7(a).

From previous characterization of TIA devices, we determined the initial parasitic capacitance of 1206 SMD resistors with 1.9 mm by 1.6 mm pads on FR-4 material to be 0.2 pF. Adjusting the values of C5 and C6 downward fits the bandwidth of the simulation to the data, then adjusting the values of C8 [in Fig. 7(a)] and C10, C11, and C14 [in Fig. 7(b)] fits the simulation curves to the observed gain peaking. For the double resistor circuit, the relative values of C10, C11, and C14 are adjusted to reflect any difference in C5 and C6 as this determines the coupling between the ground strip and the resistor body. Gain curves, real and simulated, are displayed in Figs. 8(a) and 8(b) for various values of feedback resistances. The fit between the simulated and real gain curves in Fig. 8 is sufficient to compute rms noise and SNR values, tabulated in Table II along with relevant characteristic values.

It should be noted that the fitted parasitic capacitances C5 and C6 are quite variable and reflect the disparity in coupling between the resistor body and the ground strip at the point of soldering; commercial flow-soldering rather than in-house hand-soldering would reduce this. Furthermore, lower values would be achieved with the minimum pad areas required for flow soldering. The 1206 SMA package was chosen as a good compromise between resistor height to pad gap (lower is better) and total pad area. The width of the upper ground strip was restricted to 0.6 mm as initial modeling indicated that greater widths would lead to amplifier instability. In fact, the double feedback resistor amplifier is unstable and requires a small 49 Ω resistor [R1, Fig. 7(b)] to damp out the oscillations. The resistor feedback combination of Fig. 7(b) almost meets the bandwidth requirements of the 200 fs time resolution, 100 MHz PRF, ASOPS-THz system operating at a Δf of 20 Hz discussed earlier. However,

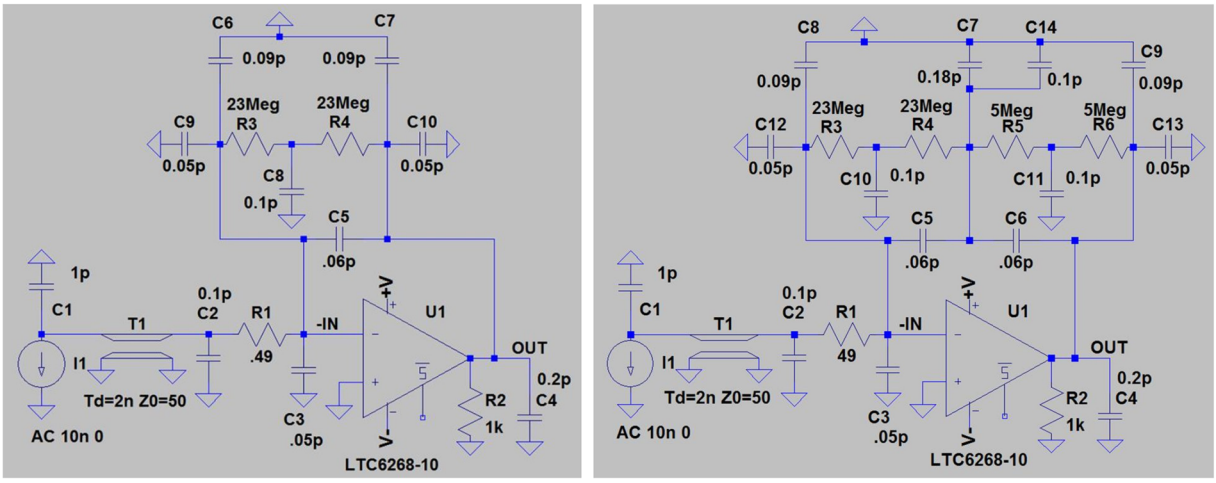


FIG. 7. Topology and initial component values for the single (a) and double (b) feedback resistor TIA.

Published under license by AIP Publishing

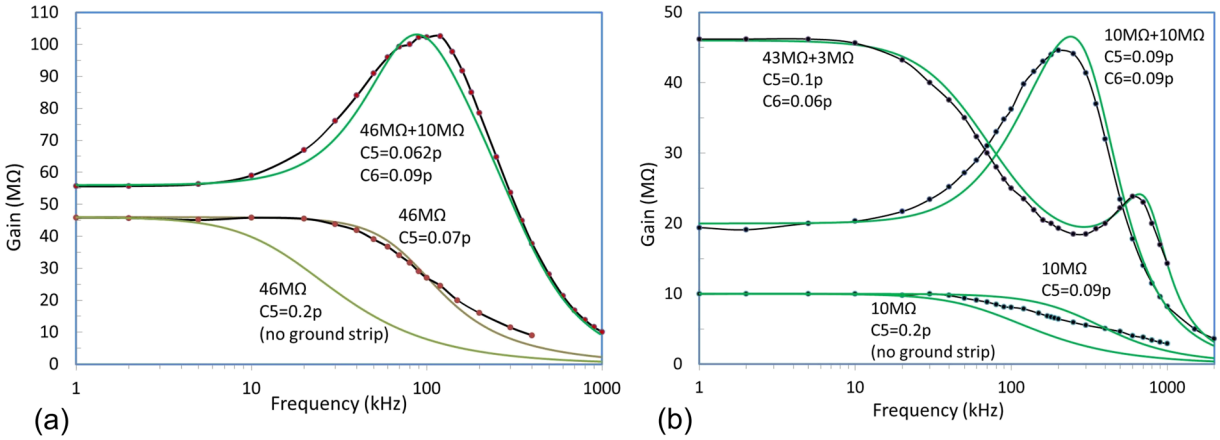


FIG. 8. Gain curves (real and simulated) for feedback resistor values: (a) 46 MΩ and 46 MΩ + 10 MΩ and (b) 10 MΩ, 10 MΩ + 10 MΩ, and 46 MΩ + 3 MΩ.

the performance of the 46 MΩ + 10 MΩ resistor feedback combination of Fig. 7(a) is examined in more detail here owing to its greater gain, in particular, to demonstrate the amplifier stability. The 43 MΩ + 3 MΩ resistor feedback combination is included in Fig. 7(b) to further demonstrate the fit between data and simulation.

The use of a ground trace under the body of the feedback resistors to reduce the parasitic feedback capacitance dramatically increases the bandwidth of the amplifiers as detailed in Table II. The 46 MΩ and 10 MΩ resistor combination increases the bandwidth from a calculated 22 MHz (R_f = 46 MΩ and C_f = 0.2 pF) to 500 MHz while delivering an additional 10 MΩ gain and a peak gain of 102 MΩ centered at 100 kHz. In general, a flat amplifier response is desired; however, for the amplification of a nonflat-top terahertz antenna source, this is not a concern and may instead be an advantage if the gain overlap is positioned to progressively increase the amplification of the weaker higher-frequency component of the terahertz signal. The SNR of this amplifier compares favorably with an amplifier of comparable bandwidth (bottom line in Table II), but the C_f value of 0.2 pF delivering an SNR of 23 dB compared with 9 dB.

IV. THz AMPLIFICATION

To assess the 46 MΩ + 10 MΩ feedback resistor TIA, a combined ASOPS and TDS THz system comprising two, identical in construction, 100 MHz pulse repetition frequency (PRF), 1550 nm wavelength, 140 fs pulse length (FWHM), fiber lasers depicted in Fig. 9 was used.[12] The emitting and receiving antenna was Batop bPCA-100-05-10-1550 and bPCA-180-05-10-1550, respectively, irradiated with 10 mW average laser power and with a 10 V dc voltage applied to the emitter. The laser offset frequency of Δf = 20 Hz was chosen to overlap the peak of the terahertz power spectrum (in scan frequency) with the peak in the amplifier gain curve, maximizing the signal to noise ratio, see Fig. 10(b). This also ensured the amplifier spectral-bandwidth of 2 THz ($1/\Delta\tau'$) was greater than the 1 THz bandwidth of the antenna combination. In comparison, in Refs. 10 and 11, the terahertz bandwidth equaled the amplifier spectral-bandwidth at a Δf of 20 Hz, where a 220 kHz, 10 MΩ TIA was employed. Finally, a 500 MHz digital oscilloscope averaged and recorded the amplified signal.

TABLE II. TIA parameters and results.

R_f (MΩ)	Gain (MΩ)	Peak gain (MΩ)	−3 dB (kHz)	rms noise (mV)[a]	SNR (dB)[b]
10 (0.2 pF)	10	...	140	5.1	
10 (data)	10	...	400	7.2	
10 + 10 (data)	20	45	900	18	15
1.5 (0.2 pF)	1.5	...	940	5.2	3
46 (0.2 pF)	46	...	22	5.2	
46 (data)	46	...	95	8.2	
46 + 10 (data)	56	102	500	20.3	23
2.8 (0.2 pF)	2.8	...	500	5.1	9

[a]rms noise calculated from fitted curves (0.1 Hz–10 GHz).
[b]SNR calculated for a ±5 nA signal.

Published under license by AIP Publishing

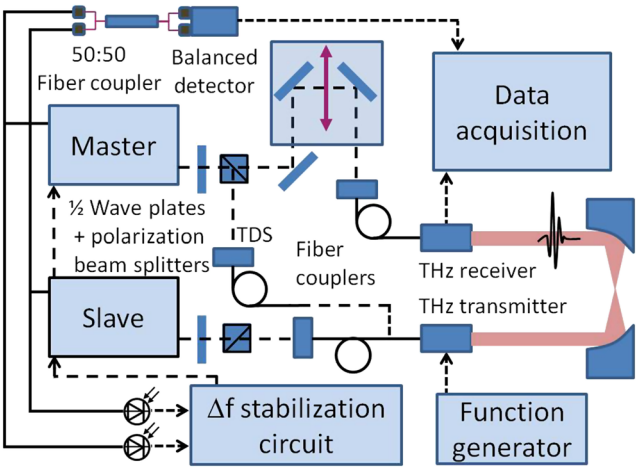


FIG. 9. Schematic of the combined THz TDS and ASOPS system.

A typical single scan ASOPS-THz signal is shown in Fig. 10(a) with the terahertz power spectrum (in scan frequency) overlaid onto the LTspice modeled gain curve of the amplifier in Fig. 10(b). Immediately of note is that the single ASOPS-THz signal is clearly visible above the noise and confers one direct advantage, no data acquisition trigger (DAT) signal is required for averaging. Furthermore, the peak signal is 700 mV and is double that expected from the 8 nA peak/peak antenna source, a direct consequence of overlapping the peak of the terahertz power spectrum (in scan frequency) with the peak in the amplifier gain curve in Fig. 10(b). It should be noted, however, that overlapping the terahertz power spectrum with the peak of the gain profile may underestimate the bandwidth limitation to the time resolution. The rms noise level detailed in Fig. 10(a) is ~35 mV, obtained from the 210 mV peak to peak noise magnitude, and agrees well with the 33 mV rms value computed from the LTspice model for the antenna fed via 1 m coax-cable length. However, this increased cable length will also reduce the amplifier bandwidth from 500 MHz to 400 MHz and peaks the gain (110 MΩ) at 95 MHz, see Fig. 10(b) and cf. Table II. In Fig. 11, the normalized power spectra are graphed for different signal averaging along with the near-frequency noise-floor values, a TDS-THz scan is included for comparison. Real time, subsecond terahertz data collection is possible at a signal to noise ratio of 30 dB. Finally, the inset of Fig. 10(a) is an overlay of a 512 averaged ASOPS-THz scan and the TDS-THz scan detailed in Fig. 11; for a full scan delay of 40 ps, no broadening of the ASOPS scan is evident compared with the one obtained via TDS.

It is instructive to examine the effect of decreasing parasitic capacitance, C_f, on the bandwidth and gain profile of the TIA as displayed in Fig. 12. To achieve a comparable bandwidth to the circuit of Fig. 7(b), a single 56 MΩ feedback resistor's C_f value must be decreased to 10 fF, an order of magnitude smaller than the 0.1 pF series combination of the 46 MΩ and 10 MΩ feedback resistors. Decreasing the value further rapidly leads to a bandwidth limitation of 500 kHz and the onset of gain-peaking, a direct consequence of Eq. (4) and the distributed 100 pF capacitance of the input cable from the receiver antenna compromising the very low value of C_{in} (0.55 pF) of the LTC6268-10 device. The broad gain peaking present in the circuit of Fig. 7(b) is due to the capacitors C7, C10, C11, and C14 progressively shunting the feedback signal to ground as frequency increases.

V. NOISE ANALYSIS, NOISE REDUCTION, AND BANDWIDTH INCREASE

The ASOPS-THz signal obtained in Fig. 10(a) is via a 1 m length 50 Ω coax cable connecting to the terahertz receiver antenna. The distributed 100 pF capacitance of this cable will add to the C_{in} value, increasing the input capacitance noise term of Eq. (3), and limit the obtainable amplifier bandwidth via Eq. (4). Of far more concern however is the large noise-peak that overlaps the gain peak and consequently the terahertz signal spectrum [Fig. 13(a)]. Removing this cable with its associated capacitance and integrating the TIA directly to the antenna will significantly reduce the total noise from the 33 mV rms level down to 7.5 mV rms and, more importantly, move the peak of the noise signal beyond the amplifier −3 dB cutoff, reducing the peak noise coincident with the terahertz signal spectrum by a factor of 20 [Fig. 13(b)]. Still present however is a significant

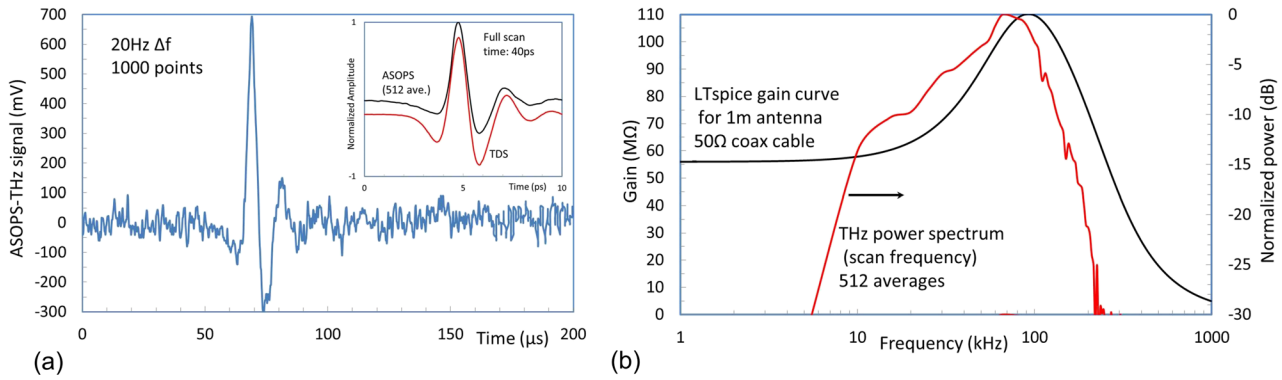


FIG. 10. (a) Single ASOPS-THz scan (inset, overlay of TDS and ASOPS scans) and (b) amplifier gain and terahertz power spectrum.

Published under license by AIP Publishing

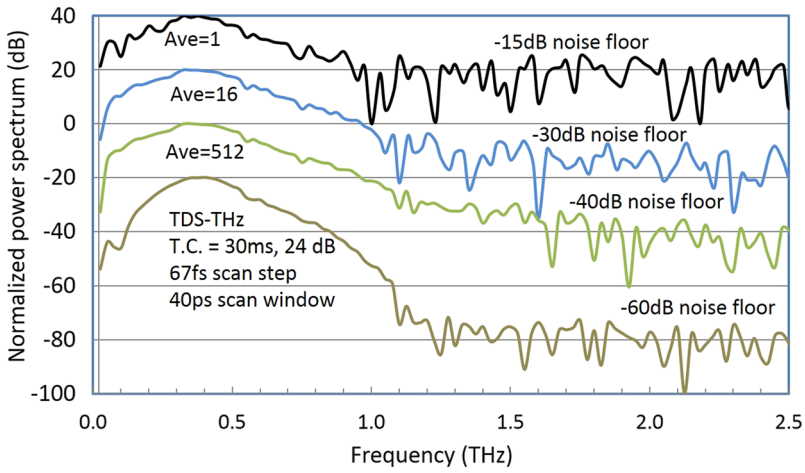


FIG. 11. Averaged ASOPS-THz power spectra. 1000 points, 200 μs scan window, and 40 ps real time scan. TDS-THz spectra, 600 points, 20 μm step, and 40 ps time scan. Note: data curves stepped by 20 dB for convenience.

noise component out to 1 GHz due to the noise signal rising steeply beyond the −3 dB amplifier cutoff but within the tail of the slow roll-off of the amplifier. Increasing the rate of this high-frequency roll-off by the addition of a low-pass-filter (e.g., active 3rd order with coincident −3 dB cutoff) will suppress this [dashed line in Fig. (13(b)], reducing the total rms noise value down to 1.8 mV and increasing the SNR figure to a very useful 52 dB. Finally, the removal of the 1 m coax cable pushes the bandwidth of the amplifier out to 550 kHz from 400 kHz.

At this point, it is useful to compare the TIA performance with the commercially available Model 312B-100 from Analog Modules.[17] The 312b-100 incorporates 100 pF input capacitance and may be directly compared to the TIA performance with a 1 m input cable. The quoted gain, bandwidth, and noise spectral density are 1 MΩ, 17 MHz, and 5.6 pA/$\sqrt{}$Hz, respectively. Restricting the noise bandwidth to 400 kHz gives a value of 3.5 nA for the rms noise input signal and an SNR of 3 dB for a 5 nA peak-current input; in comparison, the TIA delivers an SNR of 23 dB, an order of magnitude improvement. Neglecting the 110 MΩ gain-peak and assuming a flat gain of 56 MΩ, the gain-bandwidth product of the TIA is also a factor of 1.3 greater than the 312b-100.

The LTC6268-10 device is specifically designed with very low C_{in} values to obtain high bandwidth and low noise. To realize the advantage of this low C_{in} characteristic device, input capacitance must be minimized, ideally to 1 pF. This precludes the use of coaxial cable and necessitates complete integration of the detector and TIA. For photodiode based detection systems with sub-1 pF junction capacitance and strip-line topology, this is relatively straightforward but may prove more difficult for terahertz antenna systems.

The use of a ground plane under the feedback resistors of a TIA can significantly increase the bandwidth of the device by lowering the parasitic capacitance of the feedback resistors, but this comes at the cost of gain peaking due to the associated capacitance to ground. Increasing the effectiveness of this technique either by better coupling between the ground plane and the resistor body or by widening the ground-strip will only exacerbate this. The problem is the high dielectric constant (Dk ~ 9) of the resistor substrate, where a ceramic

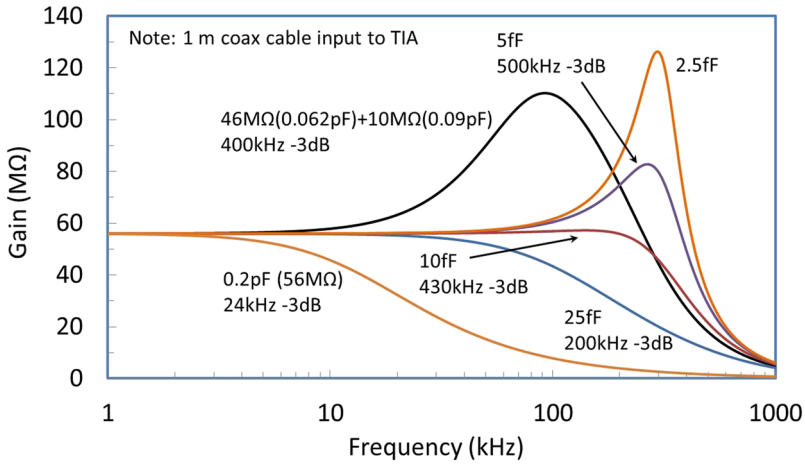


FIG. 12. LTspice modeled gain curves for a single 56 MΩ feedback resistor with decreasing values of C_f.

Published under license by AIP Publishing

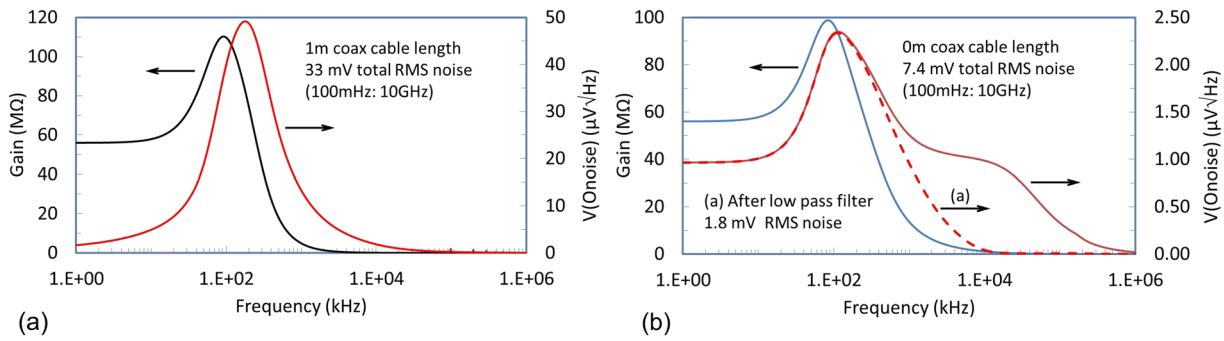


FIG. 13. Gain and V(Onoise) for the circuit of Fig. 7(b) with (a) a 1 m lead cable and (b) no cable.

material is used to ensure good power handling capabilities. For the feedback resistors in terahertz detection TIAs, this is not an issue and allows the resistor body to be fabricated out of a lower dielectric constant material. Fabricating the resistor body out of RF suitable material with Dk values below 2.5 and, in addition, using an RF suitable PCB material (Dk < 2.5) would greatly extend the bandwidth capabilities of this technique by enabling better coupled and wider ground strips to be used while reducing the initial value of C_f.

VI. CONCLUSION

The methodology has been outlined to correctly identify the high-bandwidth devices that are able to deliver the lowest noise voltage-amplification from the receiving terahertz antenna or photodiode current sources. We further show that to achieve the lowest noise levels and hence highest SNR values, amplifier input capacitance must be minimized requiring the amplifier and detection circuitry to be carefully integrated onto a single PCB. We validate a useful technique to minimize feedback parasitic capacitance, C_f, and demonstrate a TIA with a peak gain of 100 MΩ, 0.5 MHz bandwidth, and a SNR of 23 dB and outline the steps required to increase this SNR to >50 dB. Employing this TIA on a 1550 nm fiber-based ASOPS system realizes a 700 mV, 26 dB SNR, single-scan signal from the 8 nA peak/peak antenna source and removes the requirement for an additional data acquisition trigger signal. Real time, subsecond terahertz data collection is possible at a signal to noise ratio of 30 dB averaging over 16 scans. Finally, we acknowledge that the limitation of the technique to maximize the amplifier bandwidth is due to the high dielectric constant (Dk = 9) of the feedback resistor substrate, and the use of a low dielectric constant material (Dk < 2.5) would remove this.

ACKNOWLEDGMENTS

This work was supported by the National Natural Science Foundation of China (Grant Nos. 61575131, 61675138, and 61575130) and the General Projects of Science and Technology Programs of Beijing Municipal Commission of Education (Grant No. SQKM201810028004).

REFERENCES

[1]K. F. Kwong, D. Yankelevich, K. C. Chu, J. P. Heritage, and A. Dienes, "400-Hz mechanical scanning optical delay line," Opt. Lett. **18**(7), 558–560 (1993).
[2]M. Lai, "Kilohertz scanning optical delay line employing a prism array," Appl. Opt. **40**(34), 6334–6336 (2001).
[3]J. Xu and X. C. Zhang, "Circular involute stage," Opt. Lett. **29**(17), 2082–2084 (2004).
[4]P. Elzinga, F. E. Lytle, Y. Jian, G. King, and N. M. Laurendeau, "Pump/probe spectroscopy by asynchronous optical sampling," Appl. Spectrosc. **41**(1), 2–4 (1987).
[5]Y. Takagi and S. Adachi, "Sub picosecond optical sampling spectrometer using asynchronous tunable mode-locked lasers," Rev. Sci. Instrum. **70**(5), 2218–2224 (1999).
[6]T. Dekorsy, F. Hudert, R. Cerna, H. Schafer, C. Janke, A. Bartels, K. Kohler, S. Braun, M. Wiemer, and S. Mantl, "Coherent acoustic phonons in nanostructures investigated by asynchronous optical sampling," Proc. SPIE **6393**, 63930H (2006).
[7]A. Bartels, R. Cerna, C. Kistner, A. Thoma, F. Hudert, C. Janke, and T. Dekorsy, "Ultrafast time-domain spectroscopy based on high-speed asynchronous optical sampling," Rev. Sci. Instrum. **78**, 035107 (2007).
[8]R. Gebs, G. Klatt, C. Janke, T. Dekorsy, and A. Bartels, "High-speed asynchronous optical sampling with sub-50 fs time resolution," Opt. Express **18**(6), 5974–5983 (2010).
[9]O. Peters, private communication (Menlo, 2018).
[10]Y. Kim and D. Yee, "High-speed terahertz time-domain spectroscopy based on electronically controlled optical sampling," Opt. Lett. **35**(22), 3715–3717 (2010).
[11]Y. Kim and D. Yee, "High-speed high-resolution terahertz spectrometers," J. Korean Phys. Soc. **56**(1), 255–261 (2010).
[12]H. Zhang, B. Su, X. Yang, Y. Wu, J. He, C. Zhang, and D. R. Jones, "Asynchronous optical sampling data-acquisition trigger-signal derived from pulse coherence coincidence," Rev. Sci. Instrum. **89**, 113108 (2018).
[13]S. Lee, J. Lim, and J. Ahn, "Strong-field two-photon absorption in atomic cesium: An analytical control approach," Opt. Express **17**(9), 7648–7657 (2009).
[14]J. M. Roth, T. E. Murphy, and C. Xu, "Ultrasensitive and high-dynamic range two-photon absorption in a GaAs photomultiplier tube," Opt. Lett. **27**(23), 2076–2078 (2002).
[15]Texas Instruments, "Transimpedance considerations for high-speed amplifiers," Application Report No. SBOA122, 2009.
[16]C. Ciofi, F. Crupi, C. Pace, and G. Scandurra, "How to enlarge the bandwidth without increasing the noise in OP-AMP-based transimpedance amplifier," IEEE Trans. Instrum. Meas. **55**(3), 814–819 (2006).
[17]See http://www.analogmodules.com for amplifier Model 312B-100 specifications.

Published under license by AIP Publishing